APPLICATION OF SOUND SOURCE IDENTIFICATION USING CLEAN-SC TO A TURBOFAN ENGINE

Tatsuya Ishii[1], Yutaka Ishii[2], Jorgen Hald[3], Kenichiro Nagai[1], and Hideshi Oinuma[1]

[1]Japan Aerospace Exploration Agency
7-44-1 Jindaiji-higashi-machi Chofu-shi, 182-8522, Tokyo, Japan
[2]Brüel & Kjaer Japan
[3]Brüel & Kjaer SVM A/S, Denmark

ABSTRACT

Propulsion system, e. g., jet engines and rocket motors, is the intensive sound sources of aircraft and space vehicles. The authors have tried to detect the sound sources with the phased array microphones. Successful examples are the comparison of the sound source maps observed behind the mixer nozzles of a turbojet engine or at the exhaust of the launch pad model. CLEAN based spatial source coherence (CLEAN-SC) method as well as non-negative least squares (NNLS) detects sound source maps with better resolution, compared to the former approaches such as the delay and sum (DAS). This paper describes the application of CLEAN-SC techniques to a small turbofan engine, DGEN380. A foldable nine-bar array was placed at the side of the engine in the open environment. For comparison, a random-geometry array for wide band holography (WBH) was applied to the engine test during the test cell operations. The source maps by the CLEAN-SC agreed well with the results of existing methods of the DAS, WBH and NNLS, and provided better resolution in detecting sound sources. The extended CLEAN-SC, correlating a reference signal in the array with other array signals, suggested a potential of evaluating directional contribution of jet noise source.

1   INTRODUCTION

The identification of acoustic sound sources is one of the key issues for the low-noise design of propulsion systems. The Japan Aerospace Exploration Agency (JAXA) and Brüel & Kjaer (B&K) have been involved in acoustic measurements using sub-scale models and full-scale systems [1-5]. For example, an array measurement was conducted using small turbofan engines of a small jet plane. Sound sources from the jet and fans were extracted well during both ground and flight tests. In a static test of a turbojet engine, the array measurement confirmed the effect of noise suppression devices, namely, mixer nozzles. A foldable nine-bar array, located along the jet axis, succeeded in visualizing the suppressed jet noise source behind the mixer nozzles. The sound source identification agreed well with the sound pressure levels obtained in the far field of the engine. The phased array measurement also contributed in reducing the acoustic

impact on the launch vehicles. The high-speed jet of the solid rocket motors is the origin of intensive sound, not only owing to the large-scale turbulent structure but also because of the interaction of the jet plume with the launch pad structure. The array system was applied to acoustic tests using a sub-scale rocket model. The results clarified that the strength of the sound source differed based on the geometries of the extension duct. As indicated through subscale model tests, an exhaust duct, part of the launch pad of JAXA's Epsilon rocket, was redesigned and alleviated the acoustic environment around the vehicle during the first Epsilon launch.

Based on this background, further applications are planned. A series of engine tests have been started in JAXA to evaluate the acoustic and aerodynamic performances of noise reduction devices, such as mixer nozzles and acoustic liner panels [6, 7]. In place of the former turbojet engine, a smaller geared turbofan engine with a high bypass ratio was employed for future research purposes, including acoustic and aerodynamic experiments. JAXA chose a demonstrator engine, DGEN380 [8], manufactured by Price Induction in France. The first technical goal in using this engine is to measure the aerodynamic and acoustic properties of a notched nozzle [9], the jet noise suppressor of which has been jointly studied with IHI Corporation. Two engine tests were carried out using both baseline conical and mixer nozzles. One test aimed to investigate the thrust, fuel consumption, and other engine performances in the test cell. The other aimed to evaluate the acoustic characteristics in an open environment. Sound source identification using a beamforming technique is a desirable way to improve the resolution compared with the former approaches, such as the delay and sum (DAS) and non-negative least squares (NNLS).

This paper describes the various applications of beamforming techniques to a DGEN380 engine. A nine-bar foldable array by B&K was used in a noise test conducted in an open environment. To improve the resolution of the jet noise sources, an extended version of the CLEAN based spatial coherence (CLEAN-SC) method was proposed. This method, extended CLEAN-SC, utilizes one of the array microphones as a reference. The measurement results among CLEAN-SC, DAS, and NNLS are compared. Application of wideband holography (WBH) in the indoor engine tests is introduced for reference. The directional contribution estimated by the extended CLEAN-SC is compared with the conventional measurement obtained by the ground microphones in an arc centred by a nozzle.

2   BEAMFORMING TECHNIQUES

2.1 Extended CLEAN-SC

For over a decade, several deconvolution methods used to increase the resolution of the beamforming output have been developed and introduced. NNLS [10] and CLEAN-SC [11] are deconvolution methods based on delay and sum (DAS) beamforming [12]. These methods are suitable for incoherent sources, such as aerodynamic sound sources observed in the high-speed stream of jet engines or launch vehicles.

An extended CLEAN-SC method was proposed by Hald [13] to estimate and map contributions from points in a map to a reference microphone placed at the source or in the area covered by the array. A traditional referenced DAS map will show amplitudes of sources coherent with the reference signal. Standard CLEAN-SC will therefore not give a meaningful output if applied in the traditional way with a reference signal: Since the entire DAS map will be coherent with the reference signal, it will also be coherent with the beamformed signal at the DAS peak. Thus, CLEAN-SC will put a point source at the peak and allocate the entire referenced source distribution to that point. The extended CLEAN-SC algorithm, on the other hand, shows for each point in the

map the part of the reference signal coherent with the source at the map point. When the sources at the different map points are incoherent, these coherent contributions to the reference signal will be the true contributions. If a set of reference microphones are positioned in different directions from the source, extended CLEAN-SC can provide for each direction a map of the sources contributing in that direction. In the present study, a subset of the array microphones was used also as references to map the sources radiating in these directions covered by the array.

The standard CLEAN-SC deconvolution method uses the averaged cross-power spectral matrix $\mathbf{G}$, which is composed of $M \times M$ elements. A schematic view is presented in Fig. 1A. Here, M is the number of microphones of the array. Once DAS beamforming has been performed based on the matrix $\mathbf{G}$, a peak position is identified, and CLEAN-SC puts a point source at the peak position. After subtracting all signal components coherent with the peak from the matrix $\mathbf{G}$, DAS beamforming is performed using the reduced version of matrix $\mathbf{G}$. This process is repeated until the peak level becomes smaller than a threshold. The amplitudes of the point sources are equal to the averaged sound pressure across the array microphones produced by the individual peak sources. The vector, $\mathbf{p}$, of peak source contributions across the array microphones is expressed as,

$$\boldsymbol{p} = \frac{G w_k}{\sqrt{w_k^H G w_k}} \qquad\qquad (1)$$

Here, w_i is the steering vector to focus at point i, the peak of which is assumed to be at $i = k$. The extended CLEAN-SC method uses the same $M \times M$ element averaged cross-power spectral matrix $\mathbf{G}$ as the standard CLEAN-SC. Furthermore, this method requires the vector of the averaged cross spectra, $\mathbf{G_R}$, between the reference signal and the array signals (Fig. 1B). Iterations are applied in almost the same way as in the standard CLEAN-SC. Subtraction of all signal components coherent with the peak must be performed for both matrix $\mathbf{G}$ and vector $\mathbf{G_R}$. The sound pressure contribution from the peak source in the reference signal is obtained as,
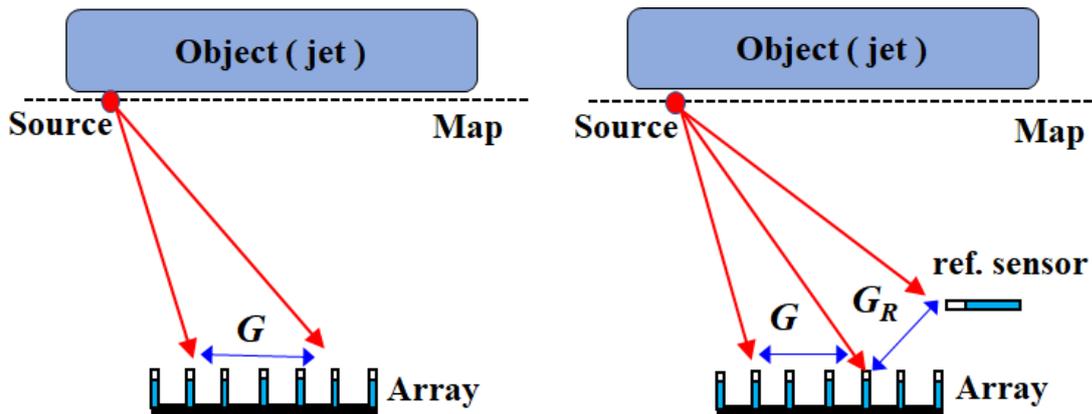
Fig. 1. Schematic view of CLEAN-SC method. The averaged cross-power spectral matrix G is obtained by array signals (left Fig. 1A). In case of extended CLEAN-SC method, the averaged cross-power spectra vector G_R is obtained by the reference signal and array signal (right Fig. 1B).

$$\boldsymbol{p_R} = \frac{G_R^H w_k}{\sqrt{w_k^H G w_k}} \qquad\qquad (2)$$

2.2 Wide Band Holography

In contrast to beamforming, near-field acoustical holography (NAH) provides a good low-frequency resolution if a sufficiently small measurement distance is used. Examples of patch-NAH methods include equivalent source method (ESM) [14] and statistically optimized near-field acoustical holography (SONAH) [15,16]. These methods work under irregular microphone array geometries, whereas the standard NAH requires regular grid arrays. As noted in references [15-17], irregular array geometries may be available in these patch-NAH methods, as well as in beamforming methods. However, the patch-NAH requires a much shorter measurement distance than beamforming.

WBH, introduced by Hald [18-20], has been proven to overcome this conflict related to the measurement distance, and provides a good resolution from low to high frequencies in a single measurement. WBH works independent of the sound source coherence. In return, the measurement distance needs to be relatively short, and the post processing time is longer because a separate processing is performed for each principal component of a measured cross-spectral matrix. In addition, at high frequencies, a sparse source distribution is assumed for the method to work.

3 ARRAY MEASUREMENT IN ENGINE TESTS

3.1 Demonstration Engine

The demonstration engine, DGEN380, is a twin-spool turbofan engine composed of a front fan with a diameter of 350 mm, a centrifugal compressor, an annular combustor, a high-pressure turbine, and a low-pressure turbine. The exhaust nozzles form a short-cowl configuration, and the bypass of the secondary nozzle ends before the core nozzle. A planetary-type gear connects the fan to the low-pressure spool and reduces the fan rotational speed. The engine is remotely controlled using the onboard engine control unit (ECU). The full authority digital engine control in the ECU enables a scheduled or automatic operation based on the spool speed or corrected spool speed. A schematic view of the engine is shown in Fig. 2, along with the representative specifications.

This engine is installed on a mechanically floating stand using a strut on the right side of the engine. The stand is suspended on a rigid stand using spring plates. The thrust received by the floating stand is transferred to the load cell unit on the rigid stand. More than 70 data points inside the engine are used to monitor the performance. The core or primary nozzle is 200 mm in diameter, including the tail cone, which is extended from the core nozzle, and thus the core nozzle forms an annular nozzle. The bypass nozzle is 460 mm in diameter. Examples of the exhaust nozzles attached to the engine are presented in Fig. 3. Because this paper deals with the beamforming techniques for jet noise, experimental results focus only on the case of a conical core and bypass nozzles. The mean velocities of the primary and secondary jets are estimated based on the total pressure and temperature profiles in the nozzles and are roughly on the order

of 290 and 170 m/s, respectively, at a low-pressure spool speed of 95%, corrected by the ambient temperature.

3.2 Measurement in Test Cell

The engine and test stand were placed in the test cell of JAXA (Fig. 4). Because the height of the rigid test stand is adjusted based on the exhaust augmenter duct, the center-line of the engine is 3 m from the floor. Although this test environment is more appropriate for evaluating the engine performance under stable atmospheric conditions than an outdoor environment, it is difficult or impossible to obtain the far field acoustic properties owing to a reverberation of the walls and other structures.

For reference, a WBH array was applied to this indoor engine operation. The array is 0.55 m in diameter and consists of five sectors within which 12 microphones are uniformly distributed. The geometry of the array and the layout of the measurement are shown in Fig. 4. Considering the diameter of the bypass nozzle, the array is outside the bypass flow, and is less affected by the very slow stream around the engine owing to the ejector effect. The array design
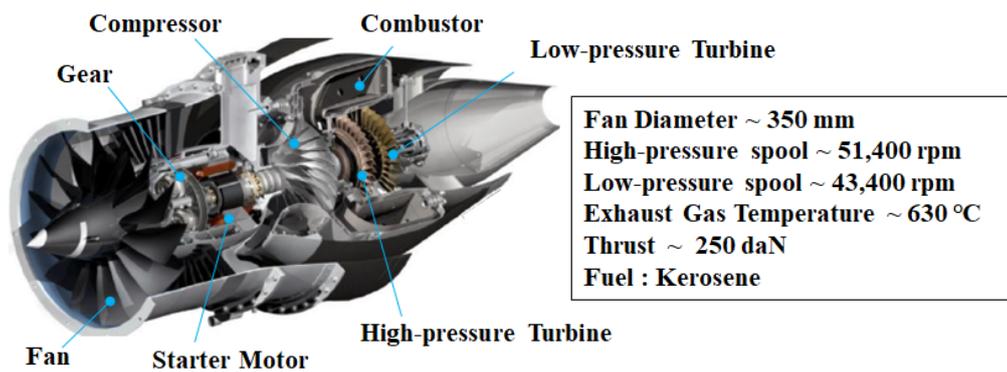
Fig. 2. Schematic view of DGEN380 geared turbofan engine and its representative specifications.
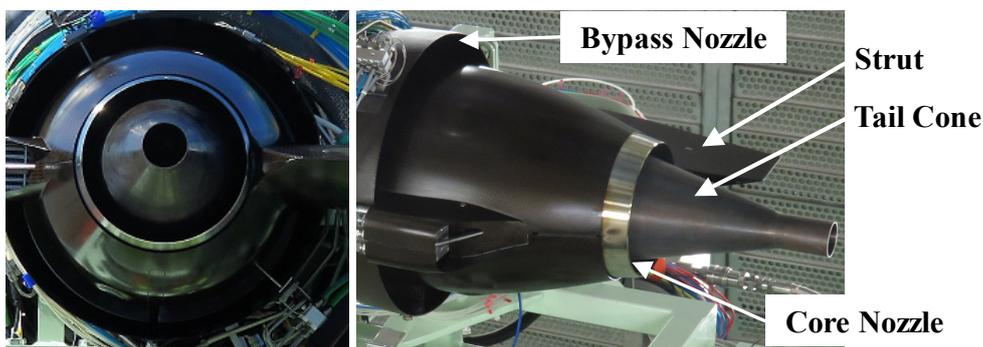
Fig. 3. Baseline nozzle applied to DGEN380 engine. Core (primary) and bypass (secondary) nozzles are conical with no mixers. As the engine is designed for a side-mounted type, at the right side of the engine is a strut to support the engine. The core nozzle was redesigned to compare the mixer nozzles.

5
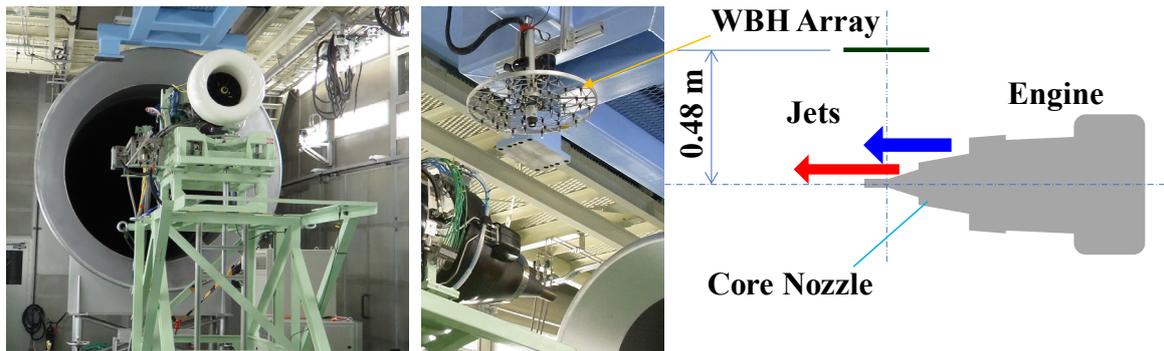
Fig. 4. WBH test setups in the test cell of JAXA. Engine, test stand and exhaust augmenter (left), WBH array above the nozzle (middle), and layout of the array (right).

follows the principle of compressive sensing, based on measurements with a random or pseudo-random array geometry. The WBH method involves the assumption of sparsity in the coefficient vector of the source model. The average element spacing is approximately 6 cm, corresponding to a beamforming measurement of up to 10 kHz. The 60-channel time signals are simultaneously stored through the B&K LAN-XI front end.

3.3   Measurement in Open Test Site

An acoustic measurement of the DGEN380 engine was conducted in the open test site of Shikabe airfield, located in the southern part of Hokkaido Japan. An overall view of the noise test is presented in Fig. 5. The base test stand is rigidly settled on a surface plate. A turbulence control system (TCS) is placed in front of the engine to reduce the atmospheric turbulence. To avoid the ground vortex, the height of the engine centerline is kept at 2 m from the surface plate, corresponding to 5.7 times the fan diameter. The fuel tank and its lined shield are on the right side in front of the engine. No other apparent acoustic obstacles are found within 50 m around the engine.

For the conventional acoustic measurements, 29 microphone stands are placed along a 20 m arc, centered by the engine inlet and nozzle exit. On the right side of the engine, the nine-bar foldable array with a diameter of 2.5 m is set in line with the jet axis. Each bar involves six microphones. The layout of the array and the engine is described in Fig. 6. In addition to a nominal analysis, this study attempts to view the directional contributions by correlating the microphone signals in the array. Seven microphones on the array were chosen as reference microphones. According to the selected reference microphones, the virtual directivity corresponds to 86° to 124° relative to the engine inlet.

The primary parameter in the measurement is the corrected low-pressure spool speed, ranging from 36% (idle) to 95%. The speed and duration are pre-determined and automatically regulated. The time duration at each speed is 180 s including the time for stabilization. The far-field acoustic data are simultaneously recorded at 51.2 kHz in the present cases. This paper refers to test case F142, which indicates the conical nozzles used in both the core and bypass nozzles. During the F142 test, the average atmospheric pressure, temperature, relative humidity, and wind speed were 102 kPa, 4.9℃, 55%, and less than 3.0 m/s, respectively.
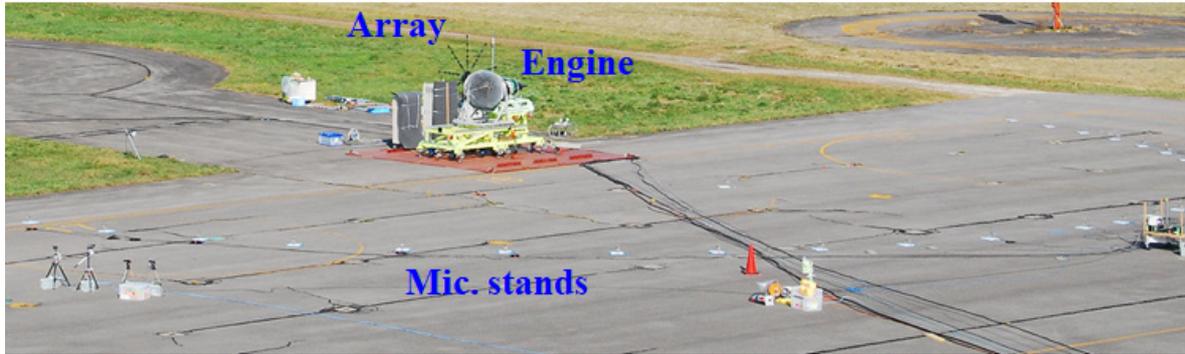
Fig. 5. Overall view of engine noise tests using DGEN380 at Shikabe airfield, Hokkaido, Japan.

F142 Conditions	
Rate	$N_{low\_corr.}$
%	[rpm]
36	16,012
70	30,573
80	34,950
90	39,328
95	41,530

Degrees	124	118	112	107	100	93	86
Ref. CH.	2	7	6	1	5	4	3
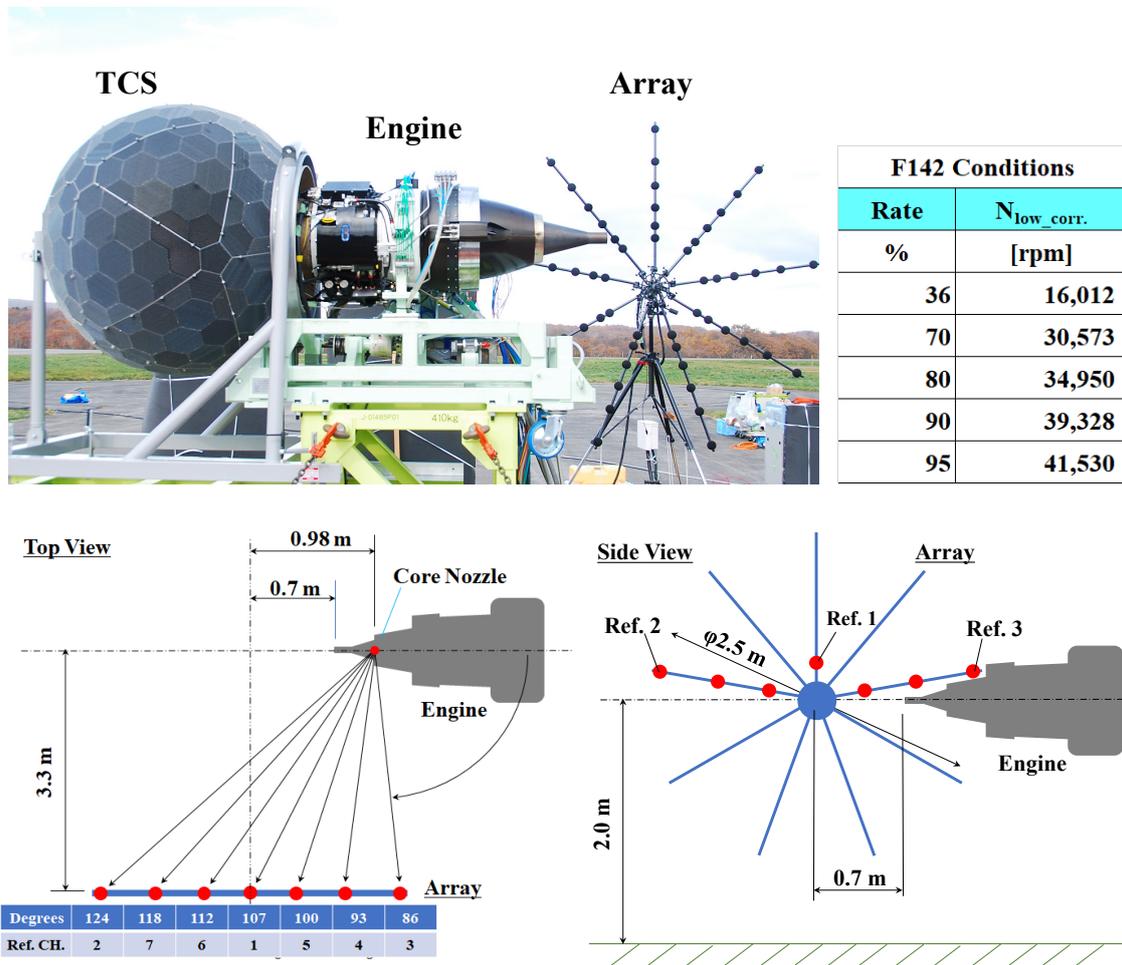
Fig. 6. Array setup in the noise tests. Engine, TCS, test stand, array (top). Layout of the 9-bar foldable array (bottom). The width of array is about 2.5 m. The farthest away reference microphone is at 1.2 times the perpendicular distance of 3.3 m.

7

4   RESULTS AND DISCUSSION

4.1   Pressure Distributions using DAS and CLEAN-SC

Analysis regions are viewed from arrays as shown in Fig. 7. Beamforming uses broader region before and after the nozzle. WBH focuses on a limited region due to the size of array and distance to the jet. Source maps from the side angle of the nozzle are compared between the DAS and CLEAN-SC in Fig. 8. According to the pressure and temperature measurement, the speeds of the core and bypass jets are estimated as 286 and 169 m/s, respectively. Both figures define three rectangular zones. The blue zone shows the region of the bypass nozzle. The green and red zones indicate the regions of the core nozzle and the far downstream zone of the nozzle, respectively.
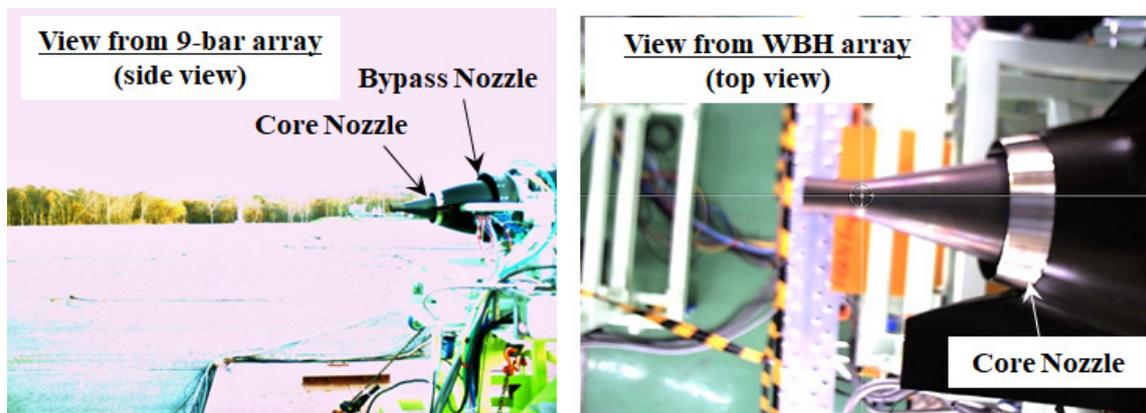
Fig. 7 Views for analysis. Side view from the 9-bar array in outdoor tests (left) and top view from WBH array in the test cell (right).
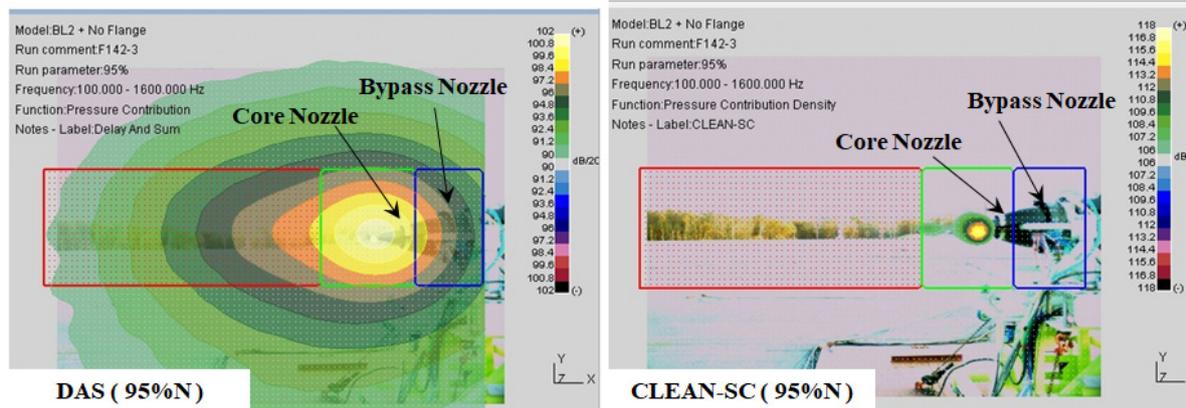
Fig. 8. Beamformed maps. Pressure contribution by DAS (left) and Pressure contribution density by CLEAN-SC (right) at 95% speed. Baseline nozzle configuration (no mixers). Broadband result covering the 1/3-octave bands 100 - 1600 Hz. Display range is 12 dB.

The frequencies for third octave bands are chosen from the 100 to 1600 Hz band. The narrow band spectra are obtained in the far field of the engine; for example, Fig. 9 points out that this engine radiates multiple types of noise in the rear directions. Dominant noise comes from tones at relatively higher frequencies of over 2000 Hz at a 95% spool speed. The tones are also dominant and involve fan, compressor, and turbine tones. Broadband noise appears at less than 2000 Hz or less, although it involves tones related to the spool speeds. At less than 100 Hz, atmospheric wind interferes with the microphones in the far-field arc, and increases the sound pressure levels.

The DAS on the left side of Fig. 8 shows the widespread distribution of the sound source. This is due to the spatial resolution being proportional to the wavelength and inversely proportional to the array diameter. Because the broadband peak frequency of the jet noise of DGEN380 is 300 to 400 Hz, the resolution of the order of 1 m in the DAS result is reasonable. The CLEAN-SC shown on the right side of the figure shows a better spatial resolution. The source positions of the DAS and CLEAN-SC are the same because the CLEAN-SC identifies point sources in the results of the DAS. CLEAN-SC iteratively replaces the peaks of the sound sources in the DAS source map with incoherent point sources. This process contributes to improving the spatial resolution [5].

When comparing to each frequency band, it is obvious that CLEAN-SC provides a much better resolution of the jet mixing noise than DAS, as shown in Fig. 10. At the band of the broadband peak, i.e., 400 Hz, CLEAN-SC predicts the existence of the sound source far downstream from the nozzle. The sound source stretched downstream is consistent with the former measurement using a turbojet engine [3]. As the center frequency increases, CLEAN-SC indicates that the position of the sound source approaches the nozzle. This shift is accounted for by the wavelength of the jet noise source associated with the turbulence scales. In contrast, DAS tends to merge the neighboring sources, and no sound sources are designated far downstream of the nozzle. This is because the incoherent point sources, assumed by CLEAN-SC, are included within a distance proportional to the DAS resolution. A set of point sources will be represented as having a smooth or spread distribution, as shown in the map of the DAS at the top of Fig. 10. In addition, the spacing between the neighboring point sources varies across the frequency bands. At lower frequencies, the DAS maps may indicate reflections on the ground surface, e.g., in the case of 200 Hz. The first identified peaks and the point sources are shifted downward from the jet axis. This shift leaves some real sources at higher positions, represented by additional point sources, and creates a contaminated or messy point source distribution.

It should be pointed out that CLEAN-SC suppresses ghost images well, as shown in the DAS maps. CLEAN-SC assumes a point source at the peak DAS position. The point source will include all side lobes associated with the real sources at the peak because the side lobes are coherent with their associated actual sources. Thus, CLEAN-SC suppresses the side lobes well by concentrating their effect on the point source.
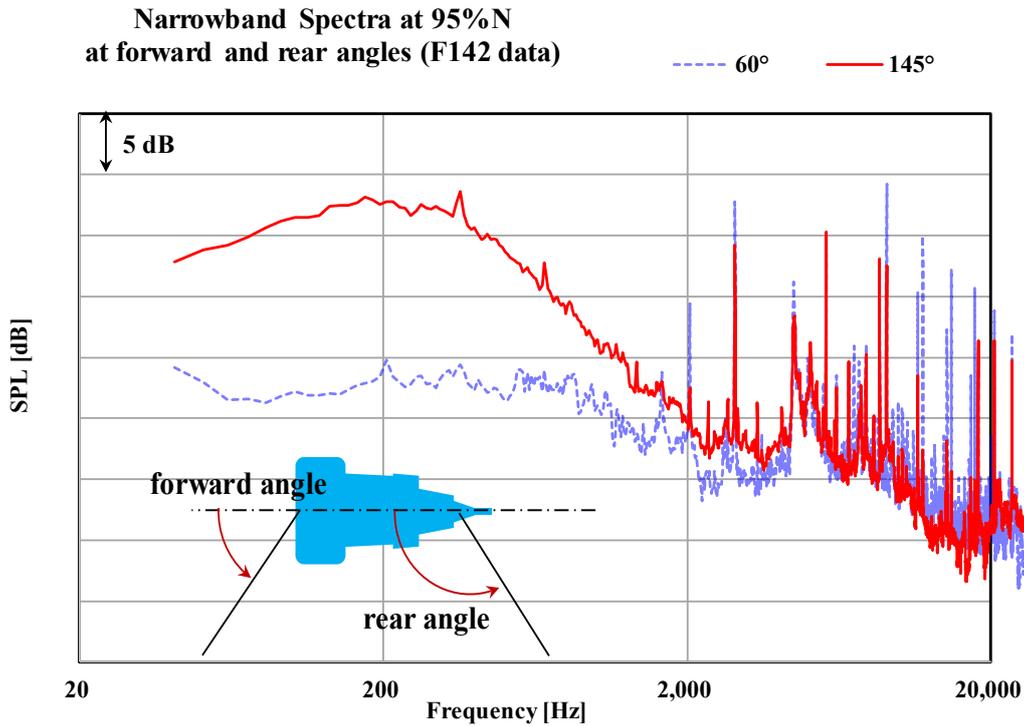
Fig. 9. Narrowband spectra in the far field of the engine at 95% speed. Third run in F142 of DGEN380 operations. Emission angles are 60° (forward angle) and 145° (rear angle).
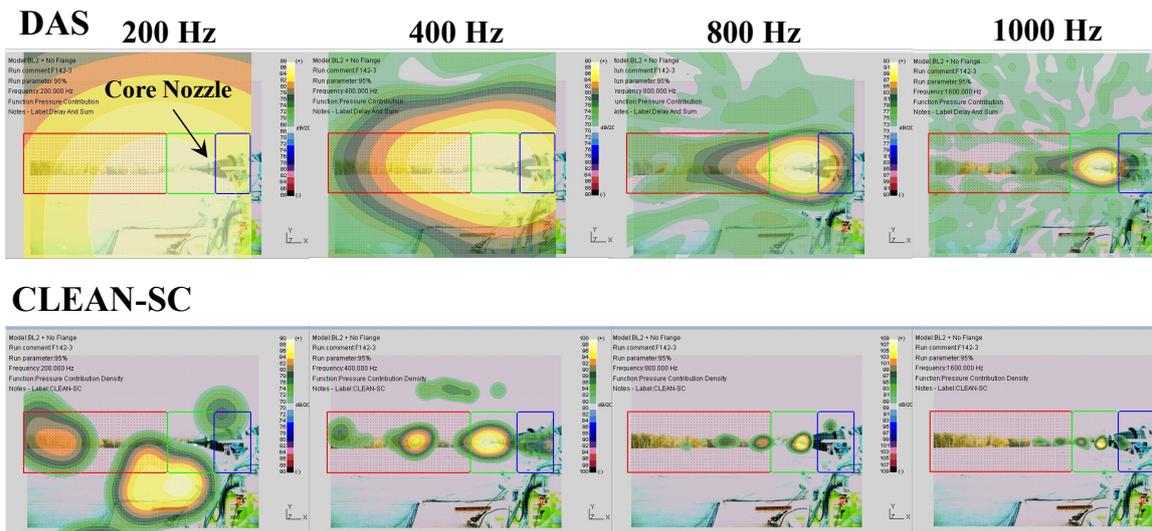
Fig. 10. Beamformed maps by DAS (top) and CLEAN-SC (bottom) at 1/3 octave bands concerned. Low-pressure spool speed is 95%.

4.2   Comparison with WBH and NNLS

The pressure distributions based on WBH resulted in similar sound sources as those by DAS, as observed in the top of Fig. 11. The peak position of the sound source moves to the nozzle end as the frequency increases, as shown in the bottom of Fig. 11. This shift in peak position is observed in CLEAN-SC maps and confirms the jet noise characteristics. However, the resolution of WBH is no better than that of DAS, partly because the distance between the array and noise sources is beyond the recommended distance, which is half of the array diameter. The acoustically reflective walls and structures in the test cell, e.g., the exhaust augmenter, are another factor deteriorating the results of WBH inside the test cell. Regardless of the worse environment, the WBH appears to provide the possibility of detecting the sound sources around the engine if appropriately applied. For comparison, an example of a sub-scale model test is presented here. A photograph of the measurement layout using the sub-scale model is shown in Fig. 12. A coaxial nozzle composed of primary and secondary nozzles emits unheated jets of Mach 0.9 and 0.5 vertically into an anechoic room of JAXA. The diameters of the core and bypass nozzles are 32 and 68 mm. The WBH array, the diameter of which is 0.55 m, was set in line with the jet axis. Although the central axis shifts slightly, the pressure distribution in the figure displays the distributed jet noise source well far behind the nozzle, which reasonably explains the jet noise levels in the nozzle's far field.

  In Fig. 13, CLEAN-SC is compared with DAS and NNLS over low frequencies between 100 and 800 Hz. As mentioned above, DAS is inferior in detecting the jet noise source stretched from the nozzle end. NNLS presents no distinct differences in source maps with CLEAN-SC. The integrated levels enclosed by rectangular zones also agree with each other within 1 to 1.5 dB at medium and higher power settings.
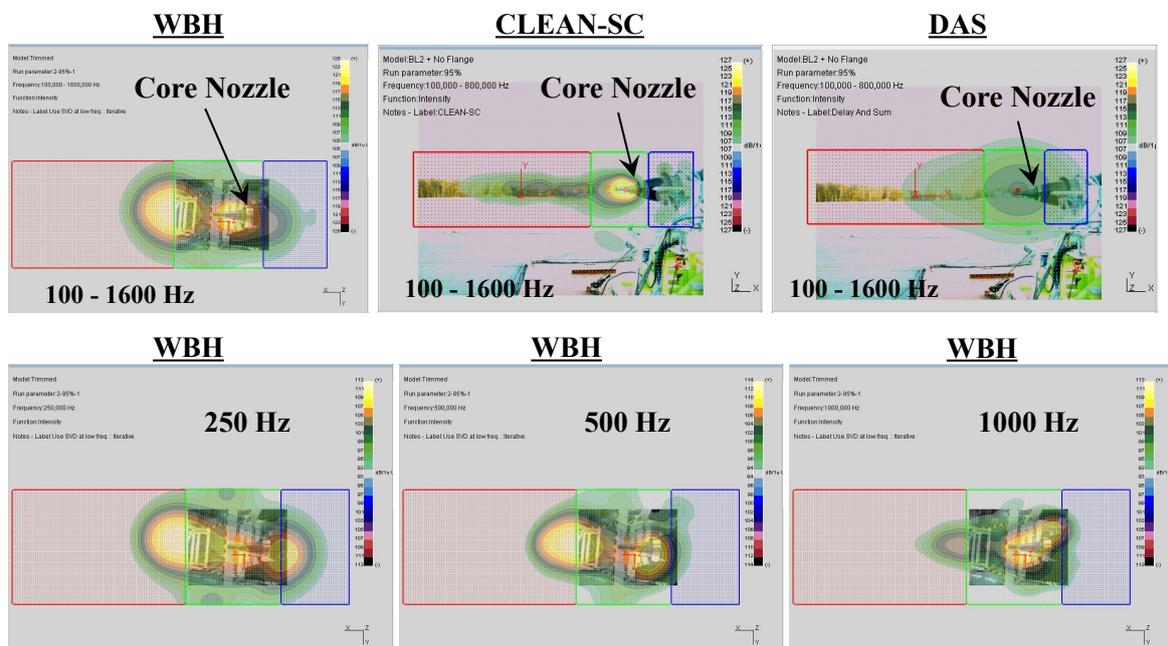
Fig. 11. Intensity maps by WBH measured in the test cell, and those by CLEAN-SC and DAS in the open test site (top). The low-pressure spool speed is 95%. Summed over 100 – 1600 Hz bands. Intensity maps at 1/3 octave bands of 250, 500 and 1000 Hz by WBH (bottom).
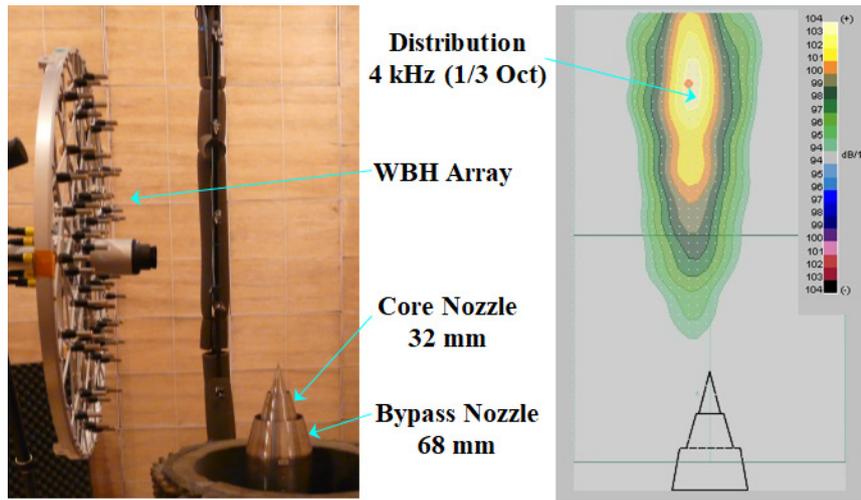
Fig. 12. Subscale model test of coaxial nozzles in an anechoic room (left). Example of WBH at 4000 Hz band (right). Core and bypass jets are kept at Mach 0.9 and 0.5 under unheated condition.
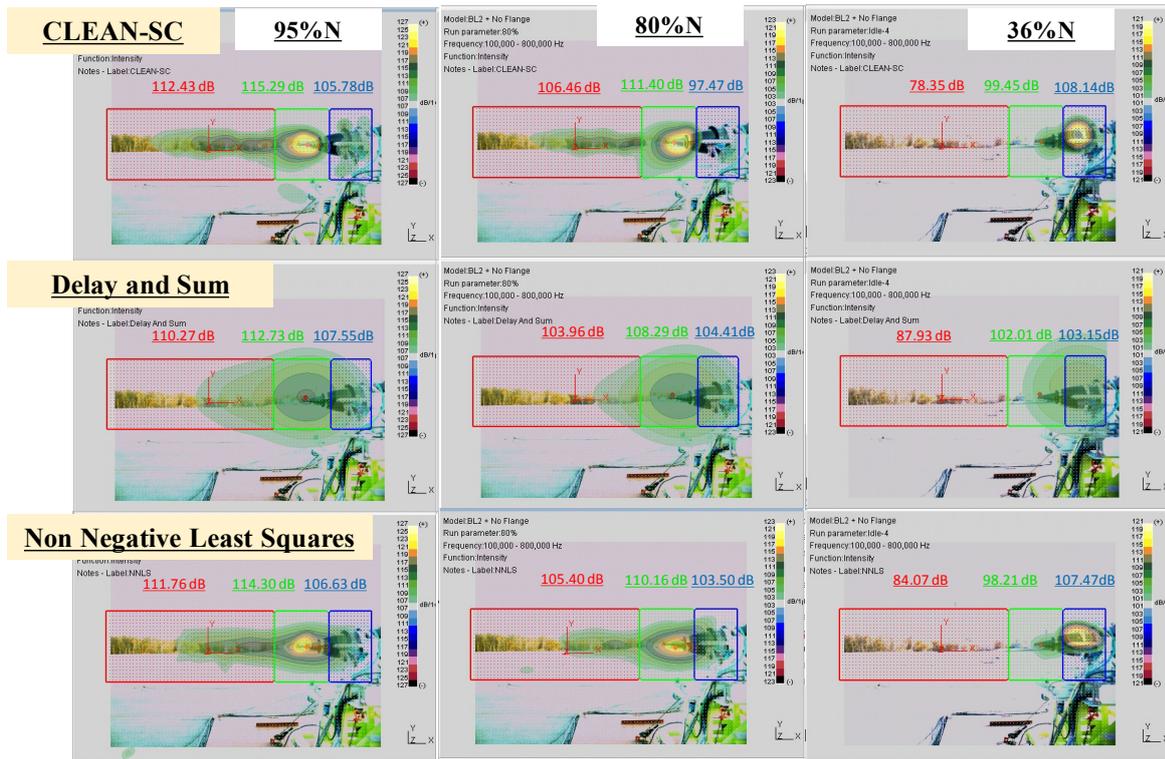
Fig. 13. Intensity maps by CLEAN-SC (top), DAS (middle) and NNLS (bottom) applied to DGEN380. The frequency bands focused are from 100 Hz to 800 Hz. The low-pressure spool speeds are 95%, 80%, and idle (about 36%).

4.3 Directional Contribution of Extended CLEAN-SC

For practical purposes, the directional contribution of the sound sources based on an array measurement would be useful. CLEAN-SC, coupled with a referential signal at a desired emission angle, is proposed in this study. This extended CLEAN-SC aims at estimating the directional source contribution relative to the emission angles. Referential microphones are chosen among the microphones in the array. Computing the correlation between the referential signal and array signals gives rise to a contribution of the noise source toward the referential microphone. It should be noted that, in the present case, the angular coverage is limited based on the size of the array, as shown in Fig. 6.

The examples of the directional contribution are shown in Fig. 14. The summed level between the 100 and 1600 Hz bands of the referential microphone, i.e., the emission angle from the engine inlet, is estimated. The low-pressure spool speed is 95%. When looking at a lower emission angle to a higher angle, the noise source expands toward the downstream and increases the level of the contribution. Thus, the summed level in the downstream zone (enclosed by the red line) gradually increases. This shift in the source map implies the influence of large-scale turbulent noise and the subsequent directional amplification of the sound pressure level in the far field of the nozzle.
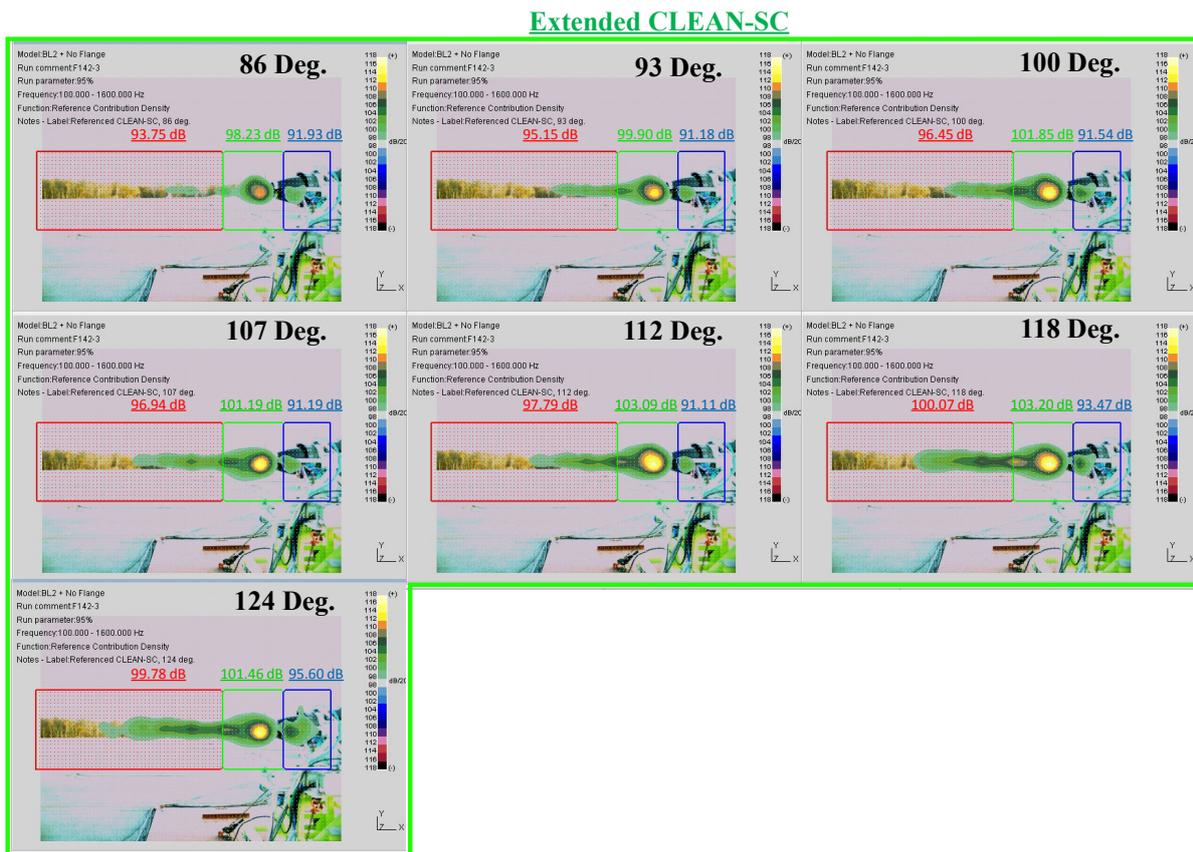
Fig. 14. Reference contribution maps, i.e., directional contribution, at several emission angles from inlet by extended CLEAN-SC (enclosed by green lines). The reference contributions might deviate from directional contributions, because the references are at different distances from the source. All data are summed from 100 Hz to 1600 Hz band when spool speed is 95%.
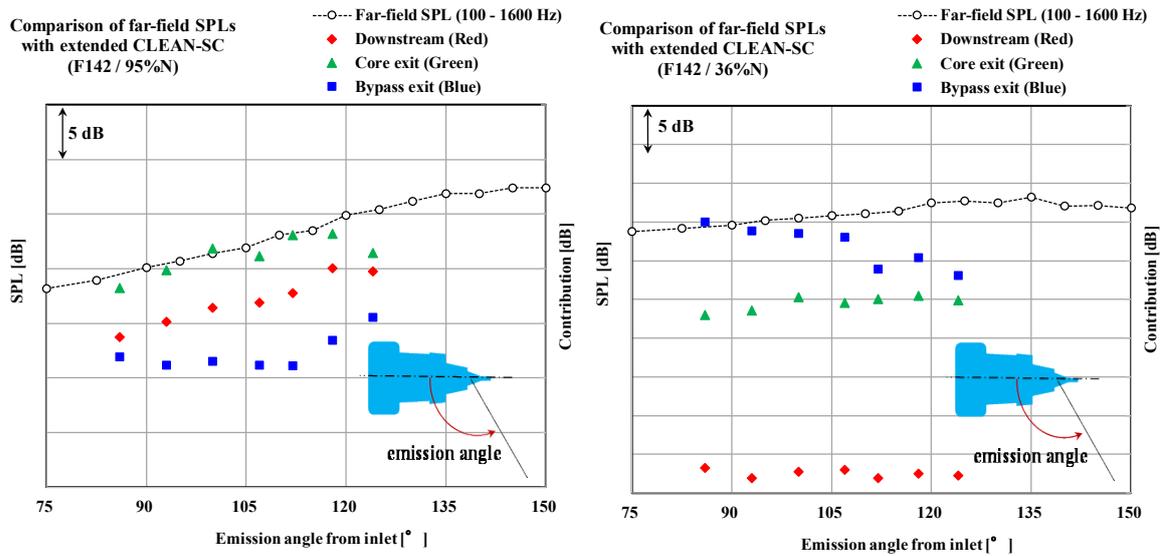
Fig. 15. Comparison of the sound pressure levels obtained in the far-field arc with results of extended CLEAN-SC. Spool speeds are 95% (left) and 36% (right). Summed level from 100 Hz band to 1600 Hz band of each zone (red, green, and blue in Fig. 14).

Figure 15 compares the results using the extended CLEAN-SC with sound pressure levels based on conventional acoustic measurements. The sound pressure levels by the far-field microphones are corrected with ground reflection and air absorption. It should be noted that the present method assumes the relative contribution and purpose to determine the directional change in the relative level. At a 95% speed, the jet noise is dominant over the concerned frequencies, and the accumulated levels slightly increase when approaching the rear angles. The representative levels around the core nozzle and far downstream by the extended CLEAN-SC appear to agree with the far-field sound pressure levels from 86° to 118° from the engine inlet. At 124°, the sum of both contributions approaches the trend of the far-field measurement, which suggests that the stretched jet noise source becomes relatively larger from this emission angle. Because the jet noise is dominant, it is natural that the sound sources around the bypass nozzle, enclosed by the blue lines, do not contribute to the far-field sound pressure levels.

As the speed of the engine decreases, the maps of the extended CLEAN-SC become similar; however, the stretched or distributed source gradually decreases and approaches the concentrated source, which leads to a change in the directional contributions. The right side of Fig. 15 compares the contributions at an idle speed, i.e., 36%. Contrary to the case of 95%, the sound source far downstream is negligible, and the far-field sound pressure level is dominated by the sound source around the bypass nozzle at shallow angles.

5   CONCLUDING REMARKS

An array was applied to a turbofan engine, namely, a DGEN380. The beamforming techniques were compared in terms of their resolution with regard to jet noise emitted from the nozzle. The following remarks were drawn:

1. In the case of jet noise at lower frequencies, while keeping the peak position the same as that of the DAS, CLEAN-SC improves the resolution and extracts sound sources hidden in the DAS source maps. In addition, CLEAN-SC agrees well with NNLS.
2. CLEAN-SC points out a similar source position as near field acoustic holography. Although the quality of WBH in the test cell was insufficient, application of the sub-scale model confirms the capability of WBH in detecting the jet noise source.
3. Under the present test case, the extended CLEAN-SC, coupled with reference microphones in an array, provides the potential for predicting the directional contribution of jet noise sources within certain emission angles.

REFERENCES

[1]   T. Ishii, K. Okai, and S. Nakamura. "Ground Tests of an Installed Jet Engine." ISABE-2013-1319, 2013.

[2]   J. Hald, Y. Ishii, T. Ishii, H. Oinuma, K. Nagai, Y. Yokokawa, and K. Yamamoto. "High-resolution Fly-over Beamforming Using a Small Practical Array." Brüel & Kjær Technical Review, No. 1(2012), pp. 1–28.

[3]   T. Ishii, N. Tanaka, T. Oishi, and Y. Ishii. "Noise Test of Revised Notched Nozzle Using a Jet Engine." ASME-GT2013-94833, 2013.

[4]   T. Ishii, S. Tsutsumi, K. Ui, S. Tokudome, Y. Ishii, K. Wada, and S. Nakamura. "Acoustic Measurement of 1:42 Scale Booster and Launch Pad." Proceedings of Meeting on Acoustics, Vol.18, 040009(2014), 2014.

[5]   Y. Ishii, T. Ishii, J. Hald, H. Oinuma, S. Tsutsumi, and K. Ui. "Application of beam-forming using deconvolution method to the development of the new launch pad of Epsilon." BeBeC-2016-D13, 2016.

[6]   T. Ishii, K. Nagai, H. Oinuma, J. Kazawa, S. Enomoto, and T. Oishi. "Preliminary Test of Turbofan Engine for Noise Research." Proceedings of International Gas Turbine Congress 2015 Tokyo, IGTC2015-0188, 2015.

[7]   T. Ishii, K. Nagai, and H. Oinuma. "Noise of small turbofan engine DGEN380." ISABE-2017-22545, 2017.

[8]   http://www.price-induction.com/

[9]   T. Oishi. "Jet Noise Reduction by Notched Nozzle on Japanese ECO-Engine Project." AIAA-2010-4026, 2010.

[10] K. Ehrenfried and L. Koop. "A comparison of iterative deconvolution algorithms for the mapping of acoustic sources." Proc 12th AIAA/CEAS Aeroacoustics Conference (27th AIAA Aeroacoustics Conference); Paper no. AIAA 2006-2711, 2006.

[11] P. Sijtsma. "CLEAN Based on Spatial Source Coherence." Proc 13th AIAA/CEAS Aeroacoustics Conference (28th AIAA Aeroacoustics Conference); Paper no. AIAA 2007-3436, 2007.

[12] D. H. Johnson and D. E. Dudgeon. "Array Signal Processing: Concepts and Techniques", Prentice Hall, New Jersey, 1993.

[13] J. Hald, H. Kuroda, T. Makihara, and Y. Ishii. "Mapping of contributions from car-exterior aerodynamic sources to an in-cabin reference signal using Clean-SC," Proc. Inter-Noise 2016, 2016.

[14] A. Sarkissian. "Method of superposition applied to patch near-field acoustical holography." J. Acoust. Soc. Am. 2005; 118(2):671–678, 2005.

[15] J. Hald. "Basic theory and properties of statistically optimized near-field acoustical holography." J. Acoust. Soc. Am. 2009; 125(4): 2105-2120, 2009.

[16] J. Hald. "Scaling of plane-wave functions in statistically optimized nearfield acoustic holography." J. Acoust. Soc. Am. 136, 2687–2696, 2014.

[17] J. Hald. "Array designs optimized for both low-frequency NAH and high-frequency beamforming." Proc Inter-Noise 2004, 2004.

[18] J. Hald. "Wideband acoustical holography," in Proceedings of Inter-Noise(2014), paper 44, 2014.

[19] J. Hald. "Extension of acoustic holography to cover higher frequencies," in Proceedings of Automotive Acoustics Conference (Autoneum) (2015), paper 20, 2015.

[20] J. Hald. "Fast wideband acoustical holography," J. Acoust. Soc. Am. 139(4), 1508-1517, 2016.